



Mechanistic implications of lanthanum-modification on gold-catalyzed formic acid decomposition under SCR-relevant conditions



Manasa Sridhar^{a,b}, Stefanie Brose^a, Dorota Siewert^a, Davide Ferri^a, Jeroen Anton van Bokhoven^{a,b,*}, Oliver Kröcher^{a,c,*}

^a Paul Scherrer Institut, Forschungsstrasse 111, CH-5232, Villigen, Switzerland

^b ETH Zurich, Institute for Chemical and Bioengineering, CH-8093, Zurich, Switzerland

^c École polytechnique fédérale de Lausanne (EPFL), Institute of Chemical Sciences and Engineering, CH-1015, Lausanne, Switzerland

ARTICLE INFO

Keywords:

Formic acid decomposition
Gold catalysis
Lanthanum-modification
C–H bond weakening
In situ DRIFTS

ABSTRACT

The use of formate-based ammonia precursors as alternatives to urea in the selective catalytic reduction (SCR) process requires that formic acid released upon their thermolysis in the hot exhaust is rapidly decomposed to carbon dioxide. This work aims at the rational development of a dedicated catalyst that is highly active and selective towards formic acid decomposition to carbon dioxide under SCR-relevant conditions, i.e. under lean conditions and in presence of a large amount of water. The incremental addition of a basic oxide (lanthana) to Au/TiO₂ revealed an optimum in the base-induced promotional effect. The base-modification of Au/TiO₂ induced a C–H bond weakening of the bidentate formates, which are the dominant surface species and the kinetically relevant intermediates for carbon dioxide formation. At 15 wt% lanthana loading, monodentate formates were substantially suppressed leading to ~85% reduction in carbon monoxide production. Very high lanthanum surface concentrations lowered the relative coverage of oxygen-derived surface species that are crucial for the decomposition of the abundantly present formates. The linearity of the Constable-Cremer relationship between the apparent activation energy and the natural log of the pre-exponential factor indicates the mechanistic similarity in formic acid decomposition on gold supported on unmodified and lanthanum-modified titania catalysts. Such mechanistic insights helped derive an optimal catalyst. The optimal catalyst exhibited close to three-fold higher activity for ammonium formate decomposition while still maintaining 100% selectivity to ammonia.

1. Introduction

The use of ammonia for the selective catalytic reduction (SCR) of NO_x in road traffic is impractical owing to the difficulty and hazards involved in the handling and storage of compressed or liquefied ammonia. For these reasons, urea is used as the ammonia source on-board vehicles. However, its usage poses several limitations [1]. This has fostered considerable interests in finding alternative ammonia precursors that are more thermally stable, freeze at lower temperatures, have higher ammonia storage capacity, and decompose more selectively. Formate-based precursors, such as guanidinium formate, ammonium formate (AmFo) and methanamide are promising candidates [2–5]. Several applications employing AmFo as an additive to aqueous urea solution demonstrate dual advantages in the form of freezing point depression and increased ammonia storage capacity [6–9]. In view of the serious problems inherent in urea-SCR [4,10], AmFo with all its

benefits appears as an attractive choice.

AmFo thermolyzes in the hot exhaust to form ammonia and formic acid [11]. While, ammonia is readily consumed by the SCR reaction, the highly corrosive and reactive formic acid must be rapidly decomposed so that it is no longer available to react with ammonia to form side products, decreasing process efficiency [10]. Moreover, selectivity to carbon dioxide rather than to carbon monoxide is of paramount importance. Previous investigations by our group revealed Au/TiO₂ to be highly active and selective under SCR conditions, i.e. in large excess oxygen and water [12]. Fresh and hydrothermally aged Au/TiO₂ exhibited no sign of deactivation with time-on-stream for 40 h in exhaust containing 5 vol% water, 10 vol% oxygen and liquid spray of 40 wt% AmFo [12,13]. The promotional effect of a basic gas phase reactant (ammonia) on the formic acid decomposition activity was realized catalytically by modification of the catalyst with lanthanum [11,13]. Formic acid decomposition proceeds via the oxidative-dehydrogenation

* Corresponding authors at: Paul Scherrer Institut, Forschungsstrasse 111, CH-5232, Villigen, Switzerland.

E-mail addresses: jeroen.vanbokhoven@chem.ethz.ch (J.A. van Bokhoven), oliver.kroecher@psi.ch (O. Kröcher).

type pathway in which active oxygen species formed from water-assisted oxygen activation facilitate the C–H bond cleavage of formate in the rate-determining-step (RDS) [14]. Moreover, under the investigated conditions, both Au/TiO₂ as well as Au/La-TiO₂ exhibited negligible WGS activity.

In this work, we systematically varied the lanthanum content to identify the optimum in the carbon dioxide production activity. Additionally, the effectiveness of two synthesis approaches to introduce lanthanum was evaluated. Kinetic and spectroscopic studies were employed to investigate the mechanistic implications of increasing lanthanum content on the decomposition activity of Au/TiO₂.

2. Experimental

2.1. Catalyst preparation

The lanthanum-modified catalysts were prepared by wet impregnation (WI) and coprecipitation (CP). In the first technique, the desired amount of lanthana is precipitated on the surface of anatase titania. The latter method by which titania and lanthana are precipitated together guarantees a more intimate contact between the two components. The wet-impregnated lanthanum-modified titania supports were synthesized in accordance with a previously published procedure [15]. An aqueous slurry consisting of calculated amounts of La(NO₃)₃·6H₂O (Fluka) and anatase titania (DT 51, Cristal Global) in 50 ml water was stirred for one hour at room temperature and then left to dry under vacuum. This was followed by a second drying step at 105 °C for 12 h. Finally, the dried powder was ground and calcined in air at 500 °C for 5 h. The coprecipitated lanthanum-modified titania supports were prepared by modifying the procedure described by Quan et al. [16]. La(NO₃)₃·6H₂O (Fluka) was dissolved in 30 ml water and subsequently added under vigorous stirring to a calculated amount of metatitanic acid TiO(OH)₂ suspension (29.97% TiO₂). The obtained solution was adjusted to pH > 9.3 using an aqueous ammonia solution (2 M NH₄OH) in order to ensure complete precipitation of the lanthanum ions and was kept under stirring for 30 min at room temperature. The precipitated solids were separated by centrifuging and washed three times with water in order to remove the ammonium ions. After drying at 105 °C for 12 h, the sample was crushed and calcined in air at 500 °C for 5 h. In order to investigate the whole range of lanthana loading, pure lanthana and titania were also synthesized in the same manner without the addition of titanium precursor and using metatitanic acid as the precursor, respectively.

The procedure for the synthesis of the gold catalysts and their testing is described elsewhere [13]. Briefly, all supports were impregnated with a 0.032 M solution of HAuCl₄ (Sigma-Aldrich), calculated on the basis of the volume of water equivalent to the pore volume of the support. The powders were aged for 1 h and washed with aqueous ammonia solution and then distilled water prior to calcination in air at 400 °C for 5 h. The gold catalysts prepared using wet-impregnated and coprecipitated supports will be henceforth referred to as AuXLT-WI and AuXLT-CP, respectively, where X denotes the wt% of lanthana. The commercial anatase (DT51) and the pure lanthana supported catalysts are designated as AuT and AuL, respectively. The titania supported catalyst prepared by using metatitanic acid as the precursor will be referred to as AuT-MA.

2.2. Activity measurements

The catalyst and the support powders were washcoated on corundite monoliths at a desired washcoat loading ($\sim 2.5 \text{ g L}^{-1}$) and tested for formic acid and ammonium formate decomposition (750 ppm each) in a dedicated setup under spray conditions [17]. Gaseous reaction products at the reactor outlet were quantified by FTIR spectroscopy (Antaris, Thermo Nicolet) [18]. The total flow rate was set at 7501 h⁻¹ and the contact time was varied by changing the number of monoliths

stacked along the length of the reactor while keeping constant the total catalyst concentration per unit volume.

2.3. Kinetic studies

For experiments determining the kinetic orders, the concentrations of formic acid, oxygen and carbon dioxide were varied in the range 200–1400 ppm, 0.25–4.00 vol% and 200–1400 ppm, respectively. External and internal mass transfer limitations were found to be negligible under the investigated conditions [13]. Conversion, product selectivity and yield were determined as described in our previous work [13]. The C-balance was closed within an accuracy of $\pm 3\%$ considering carbon monoxide, carbon dioxide and formic acid concentrations. Temperature programmed oxidation and time on stream experiments revealed that no carbon deposition occurred on the catalysts.

2.4. Catalyst characterization

A Micromeritics Tristar 3000 instrument cooled with liquid nitrogen at 77 K was used to perform nitrogen physisorption. All samples were pretreated at 150 °C for 1 h under a continuous flow of nitrogen to remove volatile impurities. The specific surface areas (SSA) were determined using the Brunauer–Emmett–Teller (BET) method. The phase composition was determined by powder X-ray diffraction (XRD) on a D8 Advance Bruker AXS diffractometer with Cu K α radiation in a 2 θ range of 10–70°. The sample composition of gold, lanthanum and titanium was analyzed by ICP-OES analysis (Varian, type VISTA Pro AX) after hot digestion in a mixture of 96% H₂SO₄ and 30% H₂O₂ (Sigma-Aldrich) and dilution in distilled water. Scanning transmission electron microscope (STEM) images were obtained on a Hitachi HD-2700 at 200 kV acceleration voltage. The catalyst powders were dispersed in ethanol and deposited onto a perforated carbon–copper grid. X-ray photoelectron spectroscopy (XPS) was performed on powder samples pressed into copper adhesive tape. The XPS chamber was kept at pressure in the order of 10⁻¹⁰ mbar during the measurement. The samples were irradiated by monochromatized Al K-alpha source at a power of 400 W. Sample charging was compensated by low energy electron flood gun. The binding energies were referenced to carbon 1 s peak from a commercial titania anatase sample at 285.25 eV (Ti2p_{3/2} at 458.85 eV). The amount of each element has been calculated from the normalized area of the respective XPS peak. Peak fitting and deconvolution was performed using UniFit 2013 (UniFit Scientific Software GmbH, Leipzig, Germany).

2.5. In situ DRIFTS measurements

The *in situ* diffuse reflectance infrared Fourier transform spectroscopy (DRIFTS) study of formic acid adsorption under steady state conditions was conducted following a previously reported procedure [13,14]. Briefly, the samples were pretreated in a flow of nitrogen containing 10 vol% oxygen and 5 vol% water at 400 °C for 0.5 h to remove any carbonate residues that may be present on the catalyst surface. After cooling the sample in flowing nitrogen to 260 °C, the background spectrum was collected. Formic acid (1120 ppm, unless otherwise stated) was dosed to the feed gas containing 10 vol% oxygen and 5 vol% water and the adsorption was monitored for 17 min. All DRIFT spectra were collected by accumulating 100 scans at 4 cm⁻¹ resolution and a scanner velocity of 80 kHz.

3. Results

3.1. Catalyst characterization

Table 1 lists the theoretical lanthanum surface coverage (La atoms nm⁻²) of all materials calculated on the basis of a simple close-packed monolayer model describing the complete dispersion of oxides and salts

Table 1

Comparison of lanthanum coverage computed on the basis of close-packed monolayer model [19,33].

Lanthana loading (wt%)	Theoretical dispersion capacity ^a (La nm^{-2})		$[\text{La}_{\text{WI}}/\text{La}_{\text{CP}}]_{\text{T}}^{\text{b}}$
	Coprecipitated	Wet-impregnated	
2.3	1.1	1.3	1.2
5	2.3	2.7	1.2
8	3.3	4.4	1.3
11	4.0	6.3	1.6
15	5.8	9.4	1.6
29	13.8	26.8	1.9
50	44.0	68.5	1.6
70	78.9	103.5	1.3

^a Assumes a simple close-packed monolayer model [19].

^b $[\text{La}_{\text{WI}}/\text{La}_{\text{CP}}]_{\text{T}}$ denotes the ratio of the theoretical lanthanum dispersion capacity of the wet-impregnated catalyst to that of the coprecipitated catalyst at a given lanthana loading.

on surfaces [19]. This model assumes that the dopant anions (O^{2-}) form a close-packed layer on the support surface while the dopant cations (La^{3+}) occupy the interstices. The ratio of theoretical lanthanum coverages of wet-impregnated and coprecipitated catalysts at a given lanthana loading, ($[\text{La}_{\text{WI}}/\text{La}_{\text{CP}}]_{\text{T}}$), is always larger than one suggesting that wet-impregnation generates higher lanthanum coverages compared to coprecipitation.

Fig. 1a and b present the XRD patterns of selected catalysts prepared by wet-impregnation and coprecipitation, respectively. The supports and the catalysts exhibited identical reflections originating primarily from the anatase phase. The very low loading (~0.5 wt%) and the high dispersion rendered the detection of gold impossible [20–22]. Irrespective of the synthesis method, increasing lanthana loading resulted in a gradual decrease in the intensity and a broadening of the anatase reflections, which are indicative of decreasing anatase crystallite size and/or higher disorder [23–28]. This is in agreement with the increase in the activation energy for nucleation and reduction in the number of nucleation sites upon coverage of lanthana on the titania grain surface [29]. With increasing lanthana loading, the anatase peaks slightly

shifted towards higher 2θ values indicating a decrease of the lattice parameter [30,31] likely as a result of peak broadening rather than an effect of La substitution in the TiO_2 lattice. This was more pronounced in the case of the coprecipitated catalysts. The large difference in the size of La^{3+} (0.115 nm) and Ti^{4+} (0.068 nm) prevents the La^{3+} from entering the lattice structure of titania; however, at the interface, a partial substitution of lanthanum atoms in the lanthana lattice by titanium atoms may occur, resulting in the formation of a Ti-O-La bond [31,32]. The resulting charge deficiency can be compensated by the formation of surface hydroxyls (Figure S1). Mixed lanthanum-titanium phases of the form $\text{La}_2\text{Ti}_2\text{O}_7$ [33,34] were present in the XRD patterns of the coprecipitated catalysts with lanthana loadings in the range $50 \leq X \leq 85$ wt%. Comparison of the broad feature in the 2θ range of 25–33° in AuXLT-WI ($X > 29$ wt%) with the reflections in the corresponding region of AuL indicates that the lanthanum phases in the wet-impregnated catalysts were present in amorphous and/or well-dispersed form. However, in the case of the coprecipitated catalysts, reflections indexed to lanthana and lanthanum hydroxide became evident in the sample with 85 wt% lanthana loading [35,36]. Lanthanum carbonates could not be identified in agreement with their high temperature of formation [37,38].

Fig. 2 shows the dependence of the anatase crystallite size from diffraction on the lanthana loading. With the introduction of only 2.3 wt% lanthana, which is equivalent to $\sim 1 \text{ La nm}^{-2}$ (Table 1), the impregnated catalysts exhibited 28% reduction in crystallite size from 25 nm to ~ 18 nm. Further addition of lanthana did not induce significant size reduction and the anatase crystallite size stabilized at ~ 14 nm at 29 wt% loading. Introduction of lanthana by coprecipitation initiated a gradual decrease of the crystallite size from the value of ~ 15 nm obtained for AuT-MA. At 29 wt% lanthana loading (Au29LT-CP), the anatase crystallite size was ~ 4 nm, which is $\sim 70\%$ lower than the average crystallite size obtained for the corresponding wet-impregnated catalyst (Au29LT-WI). As a consequence, the coprecipitated catalysts possessed higher specific surface areas than their wet-impregnated counterparts (Fig. 3). In agreement with several works [15,24,27] reporting the effect of lanthanum-modification at low loadings (< 20 wt%), the surface area of the coprecipitated catalysts

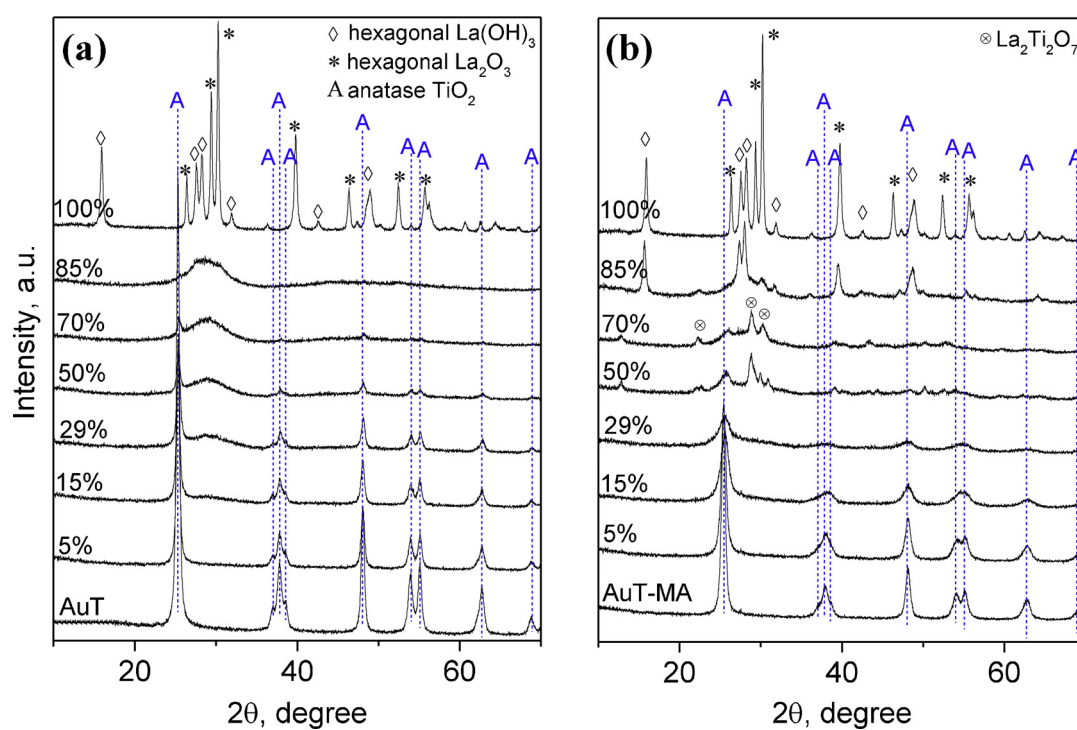


Fig. 1. XRD patterns of the lanthanum-modified catalysts prepared by (a) wet-impregnation and (b) coprecipitation.

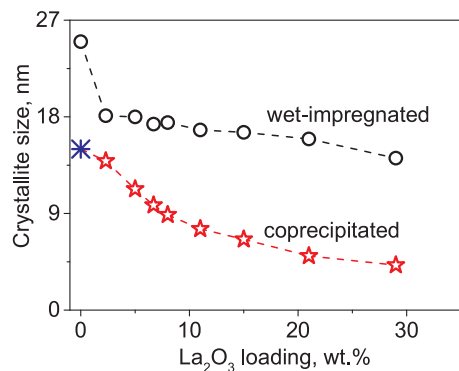


Fig. 2. Evolution of the crystallite size (nm) as a function of lanthana loading in gold catalysts prepared by coprecipitation and wet impregnation. The star represents the crystallite size of AuT-MA.

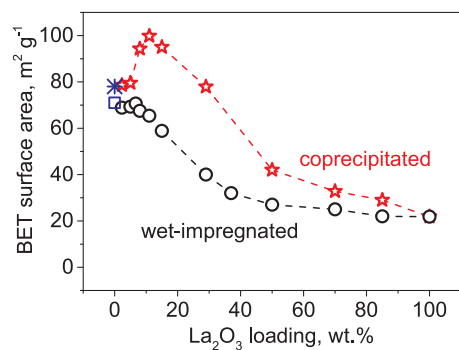


Fig. 3. BET surface area ($\text{m}^2 \text{g}^{-1}$) as a function of lanthana loading in the gold catalysts prepared via coprecipitation and wet impregnation. (□) AuT and (✳) AuT-MA.

passed through a maximum at 15 wt%. This value corresponds to a lanthanum surface density of 5.8 La nm^{-2} , which is lower than the reported monolayer coverage on titania (9.4 La nm^{-2}) [33]. Below this critical lanthanum dispersion, lanthana preferentially forms a sub-monolayer on titania, which prevents the coalescence and growth of titania crystallites [19]. At higher loadings, multilayers of lanthana and eventually phase segregation cause a reduction in surface area. In the wet impregnated catalysts, the surface area did not change significantly up to 11 wt% lanthana ($65\text{--}70 \text{ m}^2/\text{g}$), while it gradually dropped for higher values and reached $\sim 25 \text{ m}^2/\text{g}$ at 50 wt% loading.

The morphology and microstructure of selected lanthanum-modified catalysts prepared by wet-impregnation and coprecipitation were studied by high angle annular dark field scanning transmission electron microscopy (HAADF-STEM, Fig. 4). AuT-MA exhibited gold particles in the same size range (5–7 nm) as those observed in AuT [12,13]. The presence of lanthana was paralleled by a decrease in the gold particle size. The average gold particle size of Au5LT-WI and Au15LT-WI was reduced to 2–3 nm in addition to the observation of a few larger particles in the range 5–7 nm. A similar trend was observed in the coprecipitated catalysts. An increased density of surface hydroxyls with increasing lanthana loading (Figure S1) can greatly facilitate high dispersion of the gold precursor resulting in smaller gold particles [39,40]. For Au15LT-WI, the lanthana coverage was calculated to be $\sim 9.4 \text{ La nm}^{-2}$, which marks the onset of formation of lanthana multilayers on titania [33]. Energy-dispersive X-ray spectroscopy (EDXS, inset of Fig. 4) confirmed that the bright rims encapsulating the titania particles in Au15LT-WI were indeed composed of lanthanum. This sort of coating was not discernable in the case of the coprecipitated analogue (Au15LT-CP). Irrespective of the synthesis methodology, rod-like morphologies formed at lanthana loadings $\geq 70 \text{ wt\%}$. For these samples, the poor contrast between the two heavier elements, gold and

lanthanum hampers their precise identification. At these high loadings, lanthanum hydroxide and lanthana segregate to form distinct XRD phases that grow preferentially in the form of rods [41–43].

The different distribution of the lanthanum component and the different morphology of impregnated and coprecipitated samples prompted us to use X-ray photoelectron spectroscopy (XPS) to measure the lanthanum surface concentrations. Table 2 presents the atomic concentration of lanthanum measured on Au5LT and Au15LT prepared by wet-impregnation and coprecipitation. The theoretical atomic percentage of lanthanum differed significantly from the values estimated by XPS. Clearly, the wet-impregnated catalysts exhibited higher degree of surface enrichment by lanthanum showing a two-fold higher concentration compared to that of the nominal atomic percentage. Such a preferential distribution of species on the surface is commonly encountered in wet-impregnated catalysts [44–46]. In marked contrast, the coprecipitated catalysts possessed a surface lanthanum concentration that was roughly equivalent to half of the nominal values. This suggests that lanthanum was dispersed more into the bulk, such that there is a lesser extent of surface enrichment [47]. Comparison of Tables 1 and 2 demonstrates that $[\text{La}_{\text{WI}}/\text{La}_{\text{CP}}]_{\text{XPS}}$ is considerably higher than $[\text{La}_{\text{WI}}/\text{La}_{\text{CP}}]_{\text{T}}$. The significant divergence between the XPS values and the theoretical values estimated using the simple close-packed monolayer model demonstrates that the wet-impregnation generates more lanthanum on the surface of the catalysts compared to the coprecipitation even at 5 wt% lanthana loading. At 15 wt% lanthana, though the theoretical lanthanum coverages are not largely different ($[\text{La}_{\text{WI}}/\text{La}_{\text{CP}}]_{\text{T}} = 1.6$), the $[\text{La}_{\text{WI}}/\text{La}_{\text{CP}}]_{\text{XPS}}$ value indicates more than three-fold higher lanthanum concentrations on the surface in the case of Au15LT-WI. These results are in agreement with the surface coating of titania particles by lanthana in this wet impregnated sample, which is absent in the coprecipitated sample Au15LT-CP (Fig. 4). Therefore, the simple close-packed monolayer model overestimates the lanthanum dispersion capacity of the coprecipitated catalysts.

Figs. 5a and b present selected *in situ* DRIFT spectra obtained during formic acid decomposition in the presence of oxygen and water. The spectra of all the catalysts are characterized by signals in the region $1700\text{--}1300 \text{ cm}^{-1}$ (Fig. 5b) that are associated with the $\nu_{\text{AS}}(\text{OCO})$ and $\nu_{\text{S}}(\text{OCO})$ stretching modes of carboxyl groups of adsorbed formates. Various shoulders on both signals can be ascribed to the presence of both bidentate and bridged configurations and of multiple adsorption sites. The shoulder at $\sim 1670 \text{ cm}^{-1}$ is ascribed to the $\nu_{\text{AS}}(\text{OCO})$ stretching mode of monodentate formate species [48]. Besides formates, the wet-impregnated catalysts exhibited features corresponding to carbonates at ca. 1500 cm^{-1} [13], which showed little contribution on the coprecipitated catalysts. Fig. 5a depicts the spectral region of the characteristic signals of formate species corresponding to the $\nu_{\text{AS}}(\text{CO}) + \delta(\text{CH})$ combination band and the $\nu(\text{CH})$ band at 2956 cm^{-1} and 2873 cm^{-1} , respectively [13]. In both catalyst series, the signal intensified with increasing lanthana loading up to 15 wt%. The intensity gain was marginal with further loading increase. This is likely the result of the trade-off between increasing basicity and decreasing surface area. Owing to the difference in the mechanism of lanthanum addition by the two synthesis methods and the resulting different structure at identical lanthana loading, a higher density of formates was observed on the wet-impregnated catalysts exposing more lanthana on the surface (Table 1 and 2), compared to their coprecipitated analogues. Au5LT-WI and Au15LT-WI exhibited broader bands suggesting the presence of multiple adsorption geometries and thus of a heterogeneous distribution of adsorption sites. While it is dangerous to compare intensities among diffuse reflectance spectra, the gradual shift of the $\nu(\text{CH})$ mode is certainly less ambiguous. With increasing lanthana loading, the band corresponding to $\nu(\text{CH})$ progressively red shifted by 25 cm^{-1} and the high frequency $\nu(\text{CH})$ band at 2873 cm^{-1} eventually disappeared in Au37LT-WI suggesting that high lanthana loading weakened the C–H bond. This observation is substantiated by similar shifts of formate bands observed on alkali-modified platinum catalysts [49–51] and of

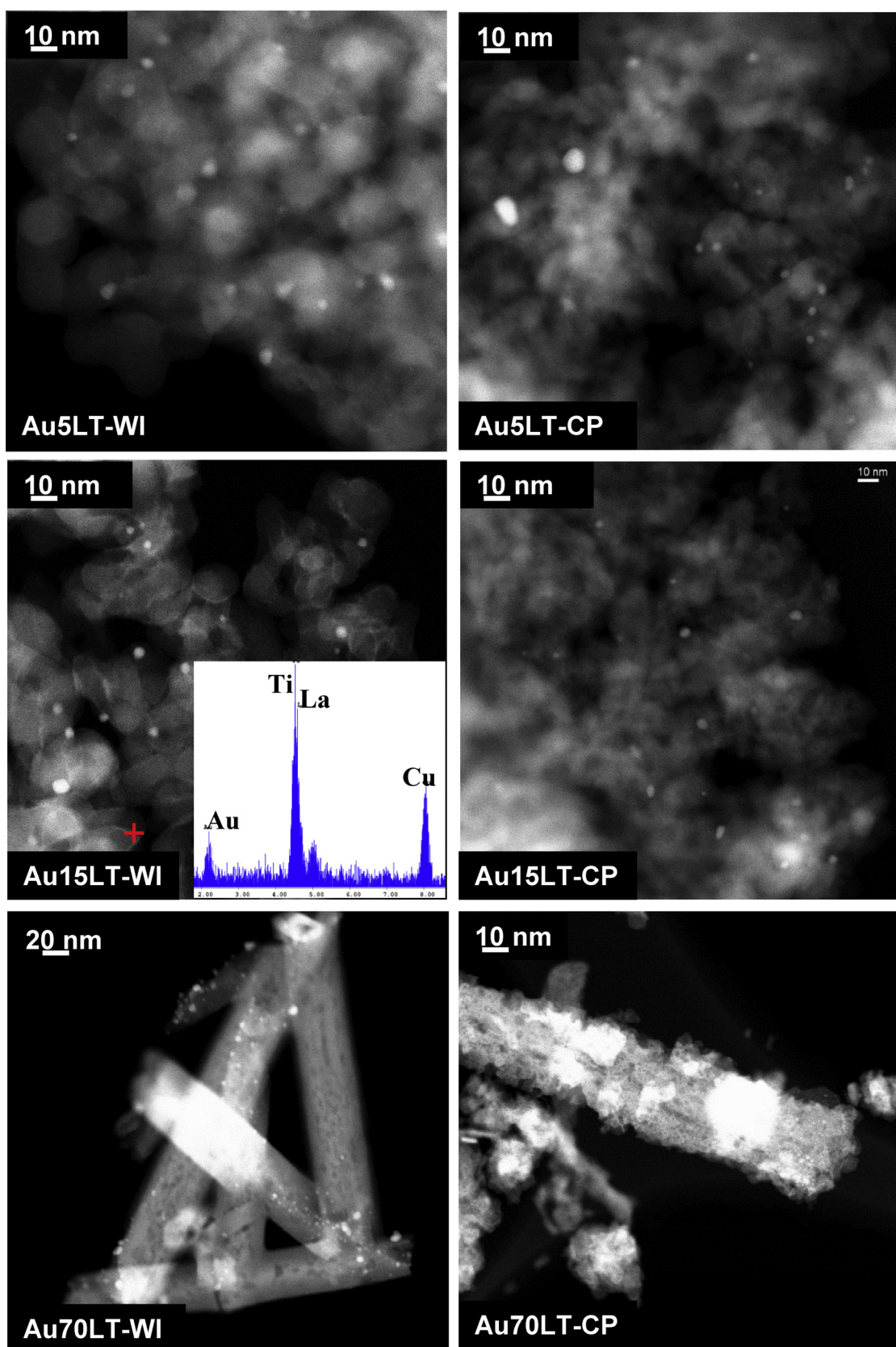


Fig. 4. HAADF-STEM images of selected gold catalysts prepared by wet-impregnation and coprecipitation.

Table 2
Estimation of surface lanthanum concentration by XPS.

Lanthana loading (wt%)	Atomic % La		$[La_{WI}/La_{CP}]_{XPS}$
	Mass-based ^a	Coprecipitated ^b	
5	0.9	0.4	1.6
15	2.6	1.3	4.4

^bcalculated on the basis of total normalized peak area of La 3d.

^b $[La_{WI}/La_{CP}]_{XPS}$ denotes the ratio of the lanthanum surface concentration of the wet-impregnated catalyst to that of the coprecipitated catalyst at a given lanthana loading determined using XPS.

^a theoretical atomic % La calculated on the basis of nominal weight % of lanthana.

methoxy species [52] coordinated to increasingly reduced oxygen vacancy sites.

3.2. Catalytic activity

3.2.1. Formic acid decomposition

High activity and selectivity for formic acid decomposition to carbon dioxide are prerequisites for the use of dedicated hydrolysis catalysts for the decomposition of alternative formate-based ammonia precursor compounds in the SCR process. Fig. 6a–d present the formic acid conversion and carbon dioxide selectivity of all catalysts at 200 °C and 300 °C. Carbon monoxide was the only other product formed at 300 °C [11–13], while it was not observed at 200 °C. Irrespective of the synthesis method, lanthana caused a sharp increase in carbon dioxide selectivity [13].

The coprecipitated catalysts exhibited significantly enhanced activity upon modification by lanthana (Fig. 6a and b). With the introduction of 2.3 wt% lanthana to AuT-MA, the formic acid conversion increased from ~18% to 24% at 300 °C along with an increase in the carbon dioxide selectivity from ~65% to ~88%. The formic acid conversion was the highest at 15 wt% lanthana loading (~56%) and the corresponding carbon dioxide selectivity was ~98%. The performance of this catalyst is similar to that of the gold catalyst prepared using a commercial lanthanum-modified titania support (10 wt% lanthana), which showed ~60% formic acid conversion and ~98% carbon dioxide selectivity [13]. Interestingly, 15 wt% lanthana corresponds to 5.8 La nm⁻², which is well below the critical loading for monolayer coverage (~10 La nm⁻²) on titania [19,33]. Beyond this optimal composition, a steady decline in formic acid conversion was observed although the carbon dioxide selectivity remained to 100%. These catalysts with lanthana loading exceeding 10 La nm⁻², suffered surface area reduction and segregation and crystallization of lanthana as evidenced from the XRD measurements and electron microscopy images. At 200 °C, a similar trend in performance was observed with the highest conversion at 15 wt% lanthana loading, which was about three-times higher than that of the unmodified catalyst.

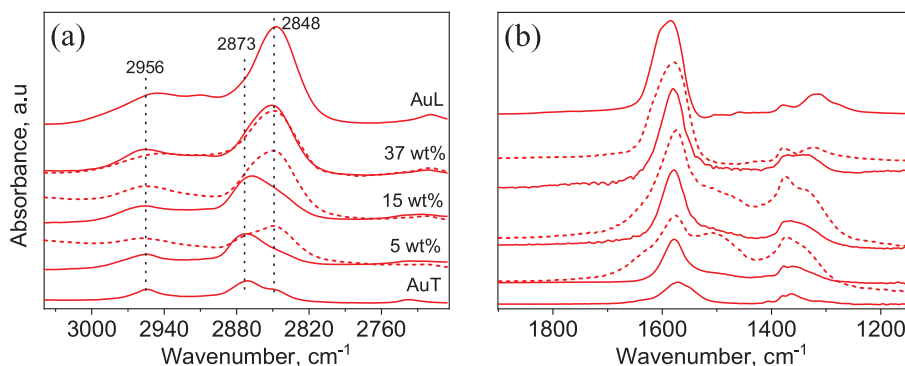


Fig. 5. *In situ* DRIFT spectra of formic acid adsorption on selected gold catalysts at 260 °C in the (a) C–H stretch and (b) carboxyl spectral ranges. Conditions: 1120 ppm formic acid, 10 vol% oxygen and 5 vol% water. Solid and dashed traces represent gold catalysts prepared by coprecipitation and wet impregnation, respectively.

The carbon dioxide selectivity of the wet-impregnated catalysts showed a very similar pattern as that of the coprecipitated ones (Fig. 6c). This was, however, accompanied by marginal changes in formic acid conversion, which remained relatively constant. The catalytic activity data indicate that lanthana addition to Au/TiO₂ catalysts suppresses carbon monoxide formation and that coprecipitation is the method of choice for preparing highly active catalysts for oxidative formic acid decomposition to carbon dioxide under SCR-relevant conditions.

3.2.2. Carbon monoxide oxidation

The carbon monoxide oxidation activity was examined to determine if carbon monoxide can be the intermediate to carbon dioxide [53,54]. Fig. 7 depicts the carbon monoxide conversion on selected catalysts in the presence and absence of water in the feed. In the presence of water, the carbon monoxide conversion remained below 5%. The carbon monoxide oxidation activity was higher by a factor of ~two in the absence of water in the feed. This observation is in line with the reported reversible poisoning of the active sites by water-derived species in a feed saturated with water vapor [13,55]. Although an increase in lanthana loading modestly increased the conversion, it only amounted to about 1/6th the carbon dioxide production from formic acid decomposition on Au15LT-CP (Fig. 6a). Therefore, the carbon dioxide produced over the lanthanum-modified catalysts originates from the direct formic acid decomposition pathway [14].

3.2.3. Formic acid decomposition on the supports

Carbon monoxide is the only product of formic acid decomposition on the pristine supports. Fig. 8 depicts the trend in carbon monoxide yield at 300 °C as a function of lanthana loading (0 ≤ X ≤ 29 wt%) in titania prepared by coprecipitation. A drop in carbon monoxide production was observed with increasing lanthana loading. The wet-impregnated catalysts behaved similarly (not shown). These results indicate that the decrease in carbon monoxide selectivity (Fig. 6) with increasing lanthana loading originates from the blockage of the acid sites on titania responsible for carbon monoxide formation [56–58].

3.2.4. Reaction orders

Fig. 9 depicts the influence of lanthana loading on the reaction orders in formic acid and oxygen. Generally, with increasing lanthana loading, the formic acid orders became more negative, while the oxygen orders became more positive. Increasingly negative formic acid orders support the activity trend at high lanthana loadings, wherein extensive poisoning of the active sites by formic acid-derived species prompts low activity. The inverse trends in formic acid and oxygen orders are consistent with a mechanism where the reaction intermediates derived from the two reactants are adsorbed at the same active site [14]. Reaction orders in carbon dioxide were close to zero, indicating that surface carbonates may exist only as spectator species.

Fig. 10 presents the ‘Constable plot’ [59,60] between the apparent activation energy (E_a) and the natural log of the pre-exponential factor (A_{app}) for formic acid decomposition on the gold catalysts with

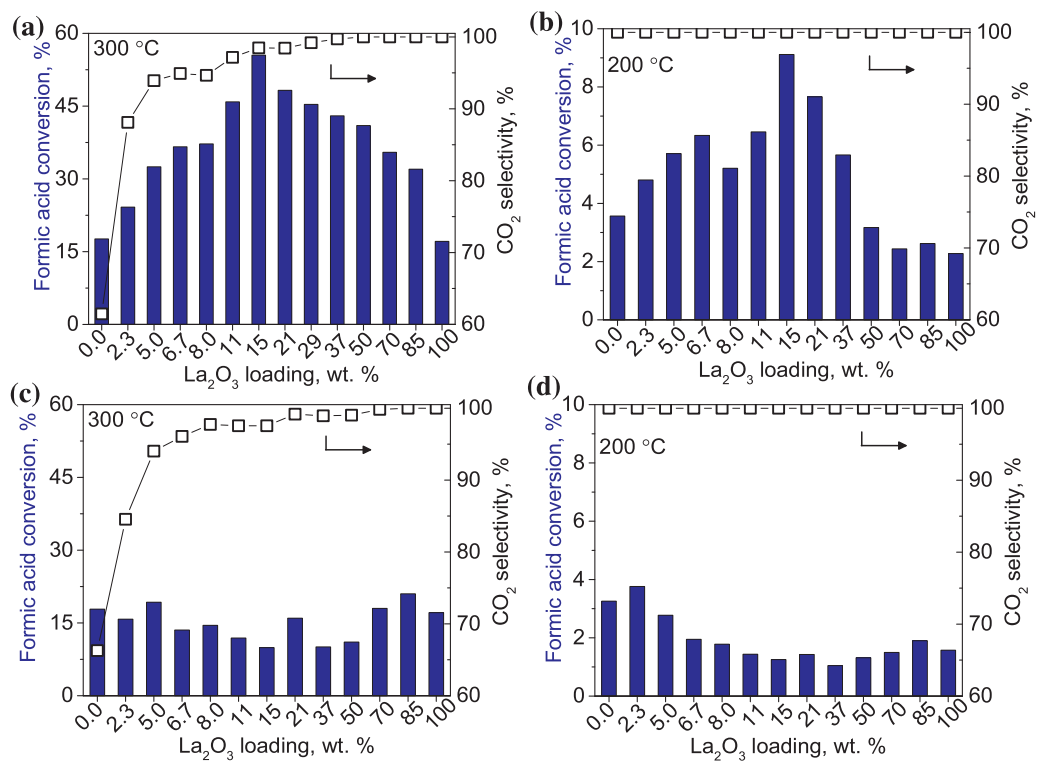


Fig. 6. Effect of lanthana loading on the performance of gold catalysts prepared via (a,b) coprecipitation, and (c,d) wet-impregnation for formic acid decomposition at 300 °C and 200 °C and W/F = 2.4×10^{-5} g s cm⁻³.

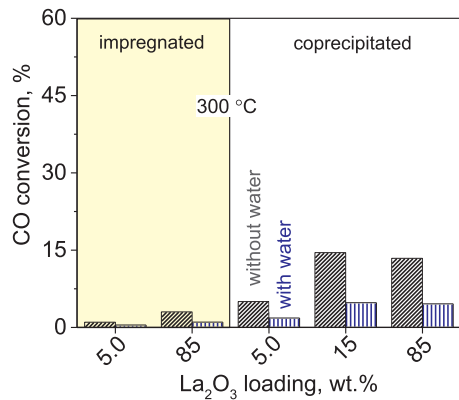


Fig. 7. Effect of lanthana loading on the performance of gold catalysts for carbon monoxide oxidation in the presence and absence of 5 vol% water in the feed at 300 °C and W/F = 7.5×10^{-5} g s cm⁻³.

increasing lanthana loading ($0 \leq X < 100$ wt%) prepared by coprecipitation. The linear relationship indicates the occurrence of the compensation phenomenon originating from systematic changes in the adsorptive properties of the catalysts without any substantial change in the overall reaction mechanism [59,60]. This is in line with the systematic change in the orders in formic acid and oxygen. The deviation of AuL indicates that a different mechanism may prevail in the absence of titania [61,62].

3.2.5. Ammonium formate decomposition

In view of the advantages outlined in the introduction, ammonium formate (AmFo) is an attractive ammonia precursor and is known to thermolyze in the gas phase to form ammonia and formic acid [10,11]. To ensure a reliable supply of ammonia for the SCR process, selectivity against ammonia oxidation is a crucial aspect in the design of a dedicated hydrolysis catalyst. To examine this, the optimal catalyst,

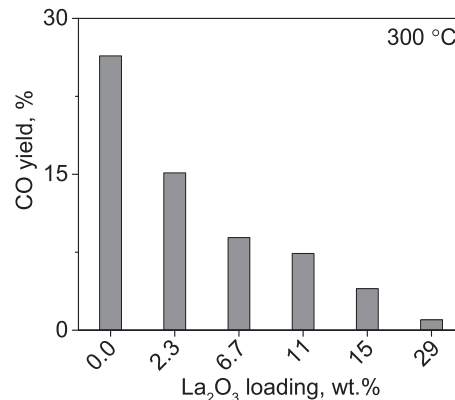


Fig. 8. Effect of lanthana loading on the performance of supports prepared by coprecipitation for formic acid decomposition at 300 °C and W/F = 2.4×10^{-5} g s cm⁻³. The supports exhibited close to zero CO₂ selectivity.

Au15LT-CP, was tested for AmFo decomposition. Fig. 11 compares the carbon dioxide and ammonia yields from the decomposition of AmFo on the unmodified and the coprecipitated catalyst with optimal lanthana loading ($X = 15$ wt%) in the temperature window 160–300 °C. The trend in the activity of the two catalysts was retained for AmFo decomposition, wherein Au15LT-CP exhibited close to three-fold higher carbon dioxide yield compared with the unmodified catalyst. The high activity of the lanthanum-modified catalyst was accompanied by nearly 100% yield of ammonia suggesting the ability of the catalyst system to efficiently decompose formic acid to carbon dioxide without consuming ammonia.

4. Discussion

In our previous study [13], we found that gold supported on commercial lanthana-modified titania exhibited enhanced selectivity for

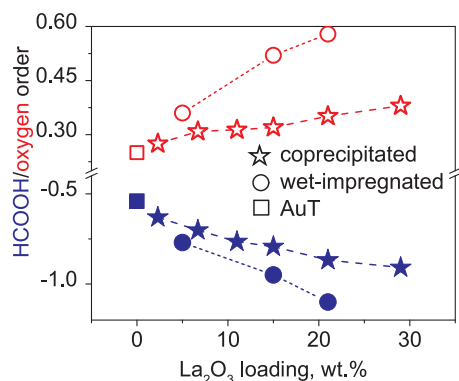


Fig. 9. Influence of lanthana loading in the gold catalysts prepared by coprecipitation and wet-impregnation on the reaction orders in (filled symbols) formic acid and (open symbols) oxygen at 300 °C and W/F = 2.4×10^{-5} g s cm⁻³.

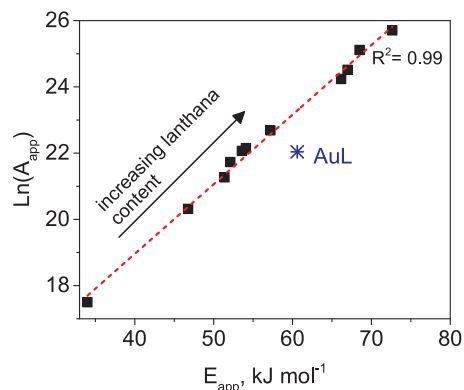


Fig. 10. Constable plot depicting the linear trend in the natural log of the pre-exponential factor (A_{app}) as a function of apparent activation energy (E_{app}) for formic acid decomposition over gold catalysts with increasing lanthana loading prepared by coprecipitation (W/F = 2.4×10^{-5} g s cm⁻³).

property of lanthanum increases the stability of molecularly adsorbed oxygen on gold, which in turn increases the concentration of the hydroperoxy species formed at interfacial Au-Ti⁴⁺ sites upon reaction with oxygen and hydrogen or water. Hence, the enhancement in the activity of the lanthana-modified catalysts can be traced back to the acceleration of the rate limiting step involving C-H bond cleavage of the formate by the hydroperoxy species.

Catalysts prepared by wet-impregnation were less active than their co-precipitated analogues. The steadily increasing concentration of lanthanum on the surface (Tables 1 and 2) bears mechanistic implications that can explain this behavior. According to the proposed single-site mechanism for formic acid decomposition under the investigated conditions [14], hydroperoxy species (OOH^*) are formed from the proton-shift equilibrium between adsorbed oxygen and water and are responsible for the decomposition of the abundantly present formates in the rate-determining-step (RDS) forming carbon dioxide. In the case of the wet-impregnated catalysts, the drastic increase in basicity originating from high surface concentrations of lanthanum results in notably higher formate coverages compared to the coprecipitated catalysts (Fig. 5). This entails an extensive blockage of the active sites by formates which in turn diminish their availability for the formation of the hydroperoxy species. This explanation is in line with the more negative order in formic acid and more positive one in oxygen.

Besides inducing an increase in the surface basicity (Fig. 5) and a decrease in the surface area (Fig. 3), an increase in the surface lanthanum coverage (Tables 1 and 2) in the case of the wet-impregnated catalysts can additionally impede the catalytic rates by reducing the interaction between gold and titania. While gold is crucial for the formation of the hydroperoxy species, tetrahedrally coordinated Ti⁴⁺ sites have been postulated to play a pivotal role in binding these species before transferring them to the active site [65,66]. Hence, the coverage of titania particles by lanthana (inset of Au15LT-WI in Fig. 4) can adversely affect the Au-Ti synergy that is responsible for the formation of hydroperoxy species.

In the proposed mechanism of formic acid decomposition under lean conditions on Au/TiO_2 [14], the dissociative chemisorption of formic acid as formate (HCOO^*) is an exothermic process while the formation of active oxygen species (OOH^*) is endothermic [67]. Hence, the formation of the former intermediate is favored at lower temperatures and the generation of the hydroperoxy species is accelerated at higher temperatures. In our previous studies, we demonstrated that the formic acid orders changed as a function of temperature and gas phase formic acid concentration, becoming less negative at lower temperature and lower formic acid concentration regime [13,14]. This is a clear sign of the measured kinetic parameters being apparent and the activation energy bearing non-negligible contributions from the heats of adsorption of the reactants. In this study, the logarithm of the pre-exponential factor (A_{app}) increases proportional to the measured (apparent) activation energy, E_{app} , which is known as the compensation phenomenon and is described by the Constable-Cremer relation (Eq. (1)):

$$\ln A_{app} = mE_{app} + c \quad (1)$$

The mechanistic reason for the compensation phenomenon is a change in the relative surface coverages of formates and hydroperoxy species, which is caused by differences in their heats of adsorption with increasing lanthana concentrations [59,68]. Bond et al. claimed that ΔE_{app} should ideally be at least 50% of the smallest E_{app} measured [59]. In our study, the value of ~52% supports the validity to the argument of the compensation phenomenon. The agreement of the results with the Constable-Cremer relation refers to an increase of the adsorption enthalpy of active-oxygen species with increasing lanthanum content, which in turn entails a higher energy barrier for their desorption [69]. This is in line with negative orders in formic acid and positive orders in oxygen.

The pre-exponential factor represents the number as well as the strength of the active sites. Overall, the observed optimum in rate

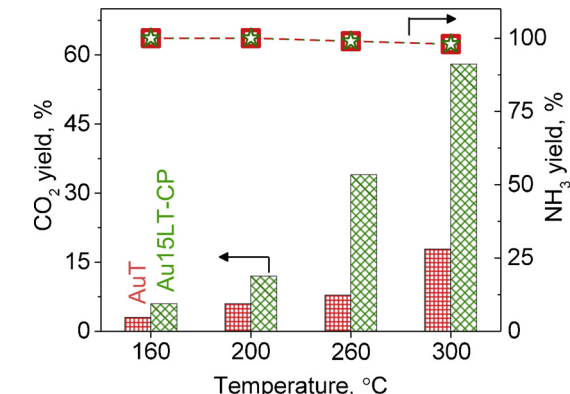


Fig. 11. Comparison of the performance of AuT and Au15LT-CP for AmFo decomposition in the temperature range 160–300 °C at W/F = 2.4×10^{-5} g s cm⁻³.

formic acid decomposition to carbon dioxide. The results of the present study indicate that lanthana addition to Au/TiO_2 resulted in enhanced formation of bidentate formates (Fig. 5b) which are the kinetically relevant precursors for carbon dioxide formation [14]. Another consequence of lanthana addition was the weakening of the C-H bond of adsorbed formates owing to the increased electron density of the catalyst, observable from the red-shift of the $\nu(\text{CH})$ band of formates (Fig. 5a) [63,64]. This red-shift reflects the catalytic effect of the base. Based on the proposed reaction mechanism mediated by hydroperoxy species (OOH^*) [14], it is reasonable to speculate that the electron-donating

enhancement by lanthana can be attributed to a favorable combination of several factors including decreased C–H bond strength of formates, increased probability of formation of hydroperoxy species arising from increased stability of adsorbed oxygen and increased number of active sites owing to the decreased gold particle size. On the other side, the highly negative formic acid orders in the case of unmodified as well as base-modified catalysts rule out the classical effect of basicity associated with an increased degree of formic acid deprotonation to formate as the most likely reason for the observed higher activity. Thus this study offers clarity on the more realistic effect of basicity on the catalytic activity for formic acid decomposition.

Modification by lanthana also favorably suppressed the carbon monoxide production. The introduction of only 1 at.% of lanthanum (corresponding to 15 wt% lanthana) to the surface of titania led to ~85% drop in formic acid conversion to carbon monoxide (Fig. 8). Monodentate formates are the intermediates relevant for carbon monoxide formation [14,64,72], which is confirmed by our study. The found decreasing trend in carbon monoxide production (Fig. 8) is correlated with a decreased tendency to form monodentate formate species with increasing lanthana loading (Figure S2). Additionally, the increased density of surface hydroxyls (Figure S1) that are engendered on the surface of lanthanum-modified titania can disfavor the RDS involving the decomposition of monodentate formate to carbon monoxide and a hydroxyl at a bridging oxygen anion [72]. These results are consistent with reports on decreased formic acid dehydration activity with increasing basicity [56,73].

5. Conclusions

In this work, we demonstrate that based on structure relations, the descriptors relevant for the design of dedicated hydrolysis catalysts exhibiting high activity and selectivity for ammonia-precursor decomposition for SCR can be identified. The basicity of titania-supported gold catalysts was tailored by incremental addition of lanthana via wet-impregnation and coprecipitation. Irrespective of the synthesis method, introduction of lanthana to Au/TiO₂ favored smaller gold particle and anatase crystallite sizes and steered the selectivity towards higher carbon dioxide production from formic acid decomposition. The rate-determining-step (RDS) involving the hydroperoxy-mediated C–H bond cleavage of formate to form carbon dioxide is assumed to be accelerated as a consequence of progressive weakening of the C–H bond as well as an increased availability of hydroperoxy species with increasing lanthana loading. However, very high surface basicity reduced the availability of active surface oxygen species owing to an extensive blockage of the active sites by formates, thus leading to a poor performance of highly basic catalysts. The systematic changes in the relative coverages of formates and hydroperoxy species lead to kinetic compensation between E_{app} and ln(A_{app}). At an optimum lanthana loading of 15 wt%, gold supported on coprecipitated lanthanum-modified titania catalyst exhibited close to three-fold enhancement in carbon dioxide production while carbon monoxide selectivity and ammonia oxidation activity were negligible. A further effect of increasing basicity was the suppression of monodentate formates which are the precursors to carbon monoxide.

Finally, we realize that aging studies in simulated SCR exhaust are needed in order for this catalyst and the ammonium formate to be an effective candidate to replace urea in practical application.

Acknowledgments

Financial support from the Swiss National Science Foundation (SNF, project number 200021_143430/1) is gratefully acknowledged. We extend our gratitude to Dr. Frank Krumeich (ETHZ) for the microscopy work.

Appendix A. Supplementary data

Supplementary material related to this article can be found, in the online version, at doi:<https://doi.org/10.1016/j.apcatb.2018.11.092>.

References

- [1] J.M. Trichard, Stud. Surf. Sci. Catal. (2007) 211–233.
- [2] O. Kröcher, P. Daniel, Ammonia Generator Converting Liquid Ammonia Precursor Solutions to Gaseous Ammonia for Denox-Applications Using Selective Catalytic Reduction of Nitrogen Oxides, WO2012104205 (A1), n.d.
- [3] A.M. Bernhard, D. Peitz, M. Elsener, O. Kröcher, Top. Catal. 56 (2013) 130–133.
- [4] M. Eichelbaum, R.J. Farrauto, M.J. Castaldi, Appl. Catal. B 97 (2010) 90–97.
- [5] A. Lundström, T. Snelling, P. Morsing, P. Gabrielson, E. Senar, L. Olson, Appl. Catal. B 106 (2011) 273–279.
- [6] A. Solla, M. Westerholm, C. Söderström, K. Tormonen, Effect of Ammonium Formate and Mixtures of Urea and Ammonium Formate on Low Temperature Activity of SCR Systems, SAE Technical Paper, (2013).
- [7] T. Nissinen, J. Kukkonen, Catalytic Process for Reducing Nitrogen Oxides in Flue Gases and Reducing Agent Composition, US7595034 B2 (2006).
- [8] M. Armin, T. Wahl, A. Ulrich, F. Brenner, M. Bareis, H. Horst, Verfahren Und Vorrichtung Zur Selektiven Katalytischen NOx-Reduktion Method and Apparatus for Selective Catalytic NOx Reduction, DE19728343 C5 (2013).
- [9] M. Koebel, M. Elsener, Ind. Eng. Chem. Res. 37 (1998) 3864–3868.
- [10] O. Kröcher, M. Elsener, E. Jacob, Appl. Catal. B 88 (2009) 66–82.
- [11] M. Sridhar, J.A. van Bokhoven, O. Kröcher, Appl. Catal. A Gen. 486 (2014) 219–229.
- [12] M. Sridhar, D. Peitz, J.A. van Bokhoven, O. Kröcher, Chem. Commun. (Camb.) 50 (2014) 6998–7000.
- [13] M. Sridhar, D. Ferri, M. Elsener, J.A. van Bokhoven, O. Kröcher, ACS Catal. 5 (2015) 4772–4782.
- [14] M. Sridhar, D. Ferri, J.A. van Bokhoven, O. Kröcher, J. Catal. 349 (2016) 197–207.
- [15] J. Zhang, Q. Xu, S. Yan, S. Zhao, C. Li, Mater. Res. Bull. 53 (2014) 3–4.
- [16] X. Quan, H. Tan, Q. Zhao, X. Sang, J. Mater. Sci. 42 (2007) 6287–6296.
- [17] D. Peitz, A. Bernhard, M. Elsener, O. Kröcher, Rev. Sci. Instrum. 82 (2011) 084101.
- [18] A.M. Bernhard, D. Peitz, M. Elsener, O. Kröcher, Top. Catal. 56 (2013) 130–133.
- [19] Y.-C. Xie, Y.-Q. Tang, in: H.P. and P.B.W.B.T.-A. in C. D.D. Eley (Ed.), Adv. Catal., Academic Press, 1990, pp. 1–43.
- [20] T. Sakwarathorn, A. Luengnaruemitchai, S. Pongstabodee, J. Ind. Eng. Chem. 17 (2011) 747–754.
- [21] X. Zhang, H. Shi, B. Xu, Catal. Today 122 (2007) 330–337.
- [22] M. Ousmane, L.F. Liotta, G. Di Carlo, G. Pantaleo, A.M. Venezia, G. Deganello, L. Retailleau, A. Boreave, A. Giroir-Fendler, Appl. Catal. B 101 (2011) 629–637.
- [23] Y. Zhang, H. Zhang, Y. Xu, Y. Wang, J. Solid State Chem. 177 (2004) 3490–3498.
- [24] Y. Liu, S. Zhou, J. Li, Y. Wang, G. Jiang, Z. Zhao, B. Liu, X. Gong, A. Duan, J. Liu, Y. Wei, L. Zhang, Appl. Catal. B 168–169 (2015) 125–131.
- [25] J. Zhang, M. Li, Z. Feng, J. Chen, C. Li, J. Phys. Chem. B 110 (2006) 927–935.
- [26] C.P. Sibu, S.R. Kumar, P. Mukundan, K.G.K. Warrier, Chem. Mater. 14 (2002) 2876–2881.
- [27] K.V. Baiju, C.P. Sibu, K. Rajesh, P. Krishna Pillai, P. Mukundan, K.G.K. Warrier, W. Wunderlich, Mater. Chem. Phys. 90 (2005) 123–127.
- [28] M.-Y. Xing, D.-Y. Qi, J.-L. Zhang, F. Chen, Chem. - A Eur. J. 17 (2011) 11432–11436.
- [29] Y.-S. Lin, C.-H. Chang, R. Gopalan, Ind. Eng. Chem. Res. 33 (1994) 860–870.
- [30] A.M. Ruiz, A. Cornet, J.R. Morante, Sensors Actuators B Chem. 111–112 (2005) 7–12.
- [31] F. Li, X. Li, M. Hou, Appl. Catal. B 48 (2004) 185–194.
- [32] Z. Hu, B. Li, X. Sun, H. Metiu, J. Phys. Chem. C 115 (2011) 3065–3074.
- [33] R. Gopalan, Y.S. Lin, Ind. Eng. Chem. Res. 34 (1995) 1189–1195.
- [34] S.D. Škapin, D. Kolar, D. Suvorov, J. Eur. Ceram. Soc. 20 (2000) 1179–1185.
- [35] Q. Mu, Y. Wang, J. Alloys. Compd. 509 (2011) 396–401.
- [36] S. Bernal, J. Diaz, R. Garcia, J.M. Rodriguez-Izquierdo, J. Mater. Sci. 20 (1985) 537–541.
- [37] B. Bakiz, F. Guinneton, M. Arab, A. Benlhachemi, S. Villain, P. Satre, J.-R. Gavarri, Adv. Mater. Sci. Eng. Int. J. 2010 (2010) 1–6.
- [38] P. Fleming, R.A. Farrell, J.D. Holmes, Ma. Morris, J. Am. Ceram. Soc. 93 (2010) 1187–1194.
- [39] P. Ganesh, P.R.C. Kent, G.M. Veith, J. Phys. Chem. Lett. 2 (2011) 2918–2924.
- [40] R. Zanella, S. Giorgio, C.R. Henry, C. Louis, J. Phys. Chem. B 106 (2002) 7634–7642.
- [41] C. Li, H. Liu, J. Yang, Nanoscale Res. Lett. 10 (2015) 1–6.
- [42] H. Zhuang, S. Zhang, X. Zhang, C. Xue, B. Li, D. Wang, J. Shen, Appl. Surf. Sci. 254 (2008) 3057–3060.
- [43] J. Ding, Y. Wu, W. Sun, Y. Li, J. Rare Earths 24 (2006) 440–442.
- [44] J.A. Navío, G. Colón, M. Macías, C. Real, M.I. Litter, Appl. Catal. A Gen. 177 (1999) 111–120.
- [45] P.G. Savva, K. Goundani, J. Vakros, K. Bourikas, C. Fountzoula, D. Vattis, A. Lycourghiotis, C. Kordulis, Appl. Catal. B 79 (2008) 199–207.
- [46] G. Li, L. Hu, J.M. Hill, Appl. Catal. A Gen. 301 (2006) 16–24.
- [47] B.M. Reddy, I. Ganesh, J. Mol. Catal. A Chem. 169 (2001) 207–223.
- [48] L.F. Liao, W.C. Wu, C.Y. Chen, J.L. Lin, J. Phys. Chem. B 105 (2001) 7678–7685.
- [49] H.N. Evin, G. Jacobs, J. Ruiz-Martinez, U.M. Graham, A. Dozier, G. Thomas, B.H. Davis, Catal. Lett. 122 (2008) 9–19.
- [50] G. Jacobs, B.H. Davis, Int. J. Hydr. Energy 35 (2010) 3522–3536.

[51] J.M. Pigos, C.J. Brooks, G. Jacobs, B.H. Davis, *Appl. Catal. A Gen.* 319 (2007) 47–57.

[52] J.S. Chung, R. Miranda, C.O. Bennett, *J. Catal.* 114 (1988) 398–410.

[53] Y.-X. Chen, M. Heinen, Z. Jusys, R.J. Behm, *Langmuir* 22 (2006) 10399–10408.

[54] M. Neurock, M. Janik, A. Wieckowski, *Faraday Discuss.* 140 (2009) 363–378.

[55] M. Haruta, *J. Catal.* 224 (2001) 221–224.

[56] M. Ai, *J. Catal.* 50 (1977) 291–300.

[57] J.M. Criado, F. Gonzalez, J.M. Trillo, *J. Catal.* 23 (1971) 11–18.

[58] X. Guo, D. Mao, G. Lu, S. Wang, G. Wu, *J. Mol. Catal. A Chem.* 345 (2011) 60–68.

[59] G. Bond, Ma. Keane, H. Kral, J. a Lercher, *Catal. Rev. Sci. Eng.* 42 (2000) 323–383.

[60] G.C. Bond, *Catal. Rev. Sci. Eng.* 50 (2008) 532–567.

[61] J.D. Lessard, I. Valsamakis, M. Flytzani-Stephanopoulos, *Chem. Commun. (Camb.)* 48 (2012) 4857–4859.

[62] M. Mihaylov, E. Ivanova, Y. Hao, K. Hadjiivanov, H. Knözinger, B.C. Gates, *J. Phys. Chem. C* 112 (2008) 18973–18983.

[63] C. Choong, Z. Zhong, L. Huang, A. Borgna, L. Hong, L. Chen, J. Lin, *ACS Catal.* 4 (2014) 2359–2363.

[64] J. Lin, K.G. Neoh, W. koon Teo, *J. Chem. Soc., Faraday Trans.* 90 (1994) 355–362.

[65] B. Chowdhury, J.J. Bravo-Suarez, N. Mimura, J. Lu, K.K. Bando, S. Tsubota, M. Haruta, *J. Phys. Chem. B* 110 (2006) 22995–22999.

[66] C.R. Chang, Y.G. Wang, J. Li, *Nano Res.* 4 (2011) 131–142.

[67] J. Huang, T. Takei, H. Ohashi, M. Haruta, *Appl. Catal. A Gen.* 435–436 (2012) 115–122.

[68] G. Bond, *Gold Bull.* 43 (2010) 88–93.

[69] Y. Zhai, D. Pierre, R. Si, W. Deng, P. Ferrin, a.U. Nilekar, G. Peng, Ja. Herron, D.C. Bell, H. Saltsburg, M. Mavrikakis, M. Flytzani-Stephanopoulos, *Science* 329 (2010) 1633–1636.

[72] M. Aizawa, Y. Morikawa, Y. Namai, H. Morikawa, Y. Iwasawa, *J. Phys. Chem. B* 109 (2005) 18831–18838.

[73] J.M. Criado, F. Gonzalez, J.M. Trillo, *J. Catal.* 23 (1971) 11–18.